Study On the Curvature of Lagrangian Trajectories in Thermal Counterflow

Naoto Sakaki[1*], Takumi Maruyama[1†] and Yoshiyuki Tsuji[1†]

[1*]Graduate School of Engineering, Nagoya University, Furo-cho, Nagoya-city, 464-8603, Japan.

*Corresponding author(s). E-mail(s): mw.41g.0347@s.thers.ac.jp;
Contributing authors: c42406a@nucc.cc.nagoya-u.ac.jp;
†These authors contributed equally to this work.

Abstract

Small particle trajectories are visualized in thermal counterflow using the particle tracking velocimetry technique, and the curvature of two dimensional Lagrangian trajectories are studied. It is found that the probability density function of the curvature demonstrates a power-law tail similar to that of classical turbulence. The curvature distribution is classified into three regions with high, medium, and low values, and the particle velocity is averaged in each region. Furthermore, the particle velocity in the low curvature region clearly shows a bimodal distribution and agrees with the two-fluid model in the case of low heat flux. However, in the high curvature region, the particle velocity deviates from the theoretical value and exhibits a Gaussian distribution. We understand from the visualized particle trajectories that the high curvature region corresponds to a complex trajectory that interacts with a quantum vortex, but the low curvature region indicates an almost straight line.

Keywords: Helium 4, Thermal counterflow, Curvature, PTV

1 Introduction

Quantum turbulence is one of the most important research fields. Thermal counterflow is a simple example of quantum turbulence. In thermal counterflow, the two-fluid velocity of helium4 demonstrates the following relation,

when considering mass conservation, $\rho_s v_s + \rho_n v_n = 0$, where ρ and v are fluid density and velocity, respectively. Moreover, the lower subscript n and s represent the superfluid and normal fluid components, respectively. The normal fluid velocity is given by Eq. (1) with a total density of $\rho = \rho_s + \rho_n$, entropy S, temperature T, and heat flux q.

$$v_n = q/\rho ST \tag{1}$$

When the relative velocity ($V = v_n - v_s$) exceeds a specific value, quantum vortices with constant circulation and a very small core of 0.1 nm are generated. Additionally, the quantum vortices are tangled in turbulence flow.

In recent years, visualization of thermal counterflow has been conducted by several researchers. Particle tracking velocimetry(PTV) or particle image velocimetry are typically adopted to calculate particle velocity. The solid hydrogen particles were used as tracer particles by Bewley *et al.* [1] to visualize the quantum vortices. Paoletti *et al.* [2] reported the probability density function (PDF) of the vertical velocity component in thermal counterflow, which has a bimodal distribution, but the horizontal component has a single peak. They are well approximated by the Gaussian distribution. Mantia *et al.* [3][4] pointed out that the PDF of velocity and acceleration have different shapes depending on the length scale, ℓ_{exp}, which is the experimental probe length or the distance between the particles along the trajectories. For example, the PDF shape exhibits an unclassical power-law tail or classical Gaussian form as the length scale increases for the horizontal velocity in thermal counterflow. In addition, the PDF tails of the horizontal acceleration, a, approach a scale of $a^{-5/3}$ as length scales decrease. Mastracci and Guo [5] developed a separation scheme for visualized particle motion. They defined three groups, namely, G1, G2, and G3. G1 group represents particles entrapped on vortices, G2 group represents untrapped particles that move relatively straight, and G3 group shows a single peak in the vertical velocity PDF. Applying this scheme shows that the PDF of transverse velocity in G1 has nonclassical features and corresponds to that of G2 shows Gaussian features. Tang *et al.* [6] proposed power-law scaling of horizontal mean-square displacement for G1 particles. It has two distinct regimes which are superdiffusion in small regions and nearly normal diffusion in large regions. According to Kubo and Tsuji [7], both regimes intersect at the transient point, which reasonably agrees to the mean intervortex distance. Švančara *et al.* [8] proposed a separation scheme of visualized particle trajectories by dividing velocity-acceleration phase space into four subspaces. They are labeled as slow (S), fast (F), acceleration, and deceleration, respectively, where S and F are related to G1 and G2, respectively. They studied the horizontal velocity PDF of S and F. Furthermore, they investigated not only PDF of S but also F having clear power-law tails as opposed to Mastracci and Guo [5]. Therefore, they concluded that not only slow particles but also fast particles are influenced by the quantum vortices when the normal velocity is large ($v_n \geq 10$ mm/s).

As noted above, previous research on thermal counterflow visualization mainly focuses on the velocity and acceleration of the tracer particles in Lagrangian properties. The curvature of tracer trajectories has not been studied in detail in thermal counterflow. In classical turbulence, particle acceleration and the curvature of Lagrangian trajectory are analyzed [9]. In magnetic turbulence, the curvature of the magnetic field line is analyzed [10] in a two-dimensional (2D) magneto hydro dynamic (MHD) turbulence. These investigations revealed that the PDF of curvature has an apparent power-law tail shape.

The thermal counterflow characteristics for helium are different from classical turbulence and MHD turbulence. In particular, the PDF varies and often exhibits a bimodal distribution, but the PDF of classical turbulence in homogeneous isotropic turbulence (HIT) closely resembles a Gaussian distribution. It is also assumed that the Lagrangian trajectories of small particles show different characteristics in quantum and classical turbulence. However, the PDF of the curvature has the same power-law tails in the thermal counterflow [11]. Moreover, trajectory of the particle can rapidly change before and after the particles are trapped by the quantum vortex. Therefore, characterizing this process by geometrical information of curvature is interesting. In addition, other physical quantities, such as velocity can be investigated in the region where the curvature is high for further analysis.

In this study, we analyzed the motion of solid hydrogen particles in thermal counterflow using the PTV algorithm. Here, we do not classify the particle size because the curvature PDF does not depend on the particle size [11], although the PDF of vertical velocity depends on the particle size [7]. The relation between the particle velocity and curvature of trajectories is studied by conditional sampling. Moreover, the particle velocity conditioned by high and low curvature regions is compared with the velocity of the two-fluid model. Finally, the interaction between the quantum vortex and the tracer particles is discussed.

2 Experiments

Figure 1 shows a schematic of the experimental setup. The acrylic rectangular channel is set inside the cryostat [11]. The channel cross-section has an area of $A = 20 \times 20$ mm^2 and a height of $H = 260$ mm. The bath temperature T varies from 1.9 to 2.1 K. Furthermore, the plate heater is located at the bottom, and the heat flux q is varied in the range of $300 - 800$ W/m^2. The thermal counterflow is generated inside the channel, and the experimental conditions are listed in Table 1. Bath temperature and heat current are included in the range of [2] and [12]. A high-speed camera (1024×1024 pixels, 8 bit) is used for visualizing the area of 8.7×8.7 mm^2 at 250 fps. A continuous laser (wavelength 532 nm, diode-pumped solid-state laser and 4 W at maximum power) is adopted to make the laser sheet with a thickness of about 1 mm. A helium and hydrogen mixing chamber is designed to vary the mixing ratio and the

Table 1: Experimental parameters; temperature T, heat current q, number of datasets, theoretical normal fluid velocity v_n, and theoretical superfluid velocity v_s.

T	q	Number of datasets	v_n	v_s
1.9 K	≈ 800 W/m^2	11	3.99 mm/s	-2.88 mm/s
2.0 K	≈ 300 W/m^2	3	1.07 mm/s	-1.32 mm/s
2.0 K	≈ 400 W/m^2	5	1.43 mm/s	-1.77 mm/s
2.0 K	≈ 800 W/m^2	13	2.86 mm/s	-3.53 mm/s
2.1 K	≈ 800 W/m^2	3	2.07 mm/s	-5.91 mm/s

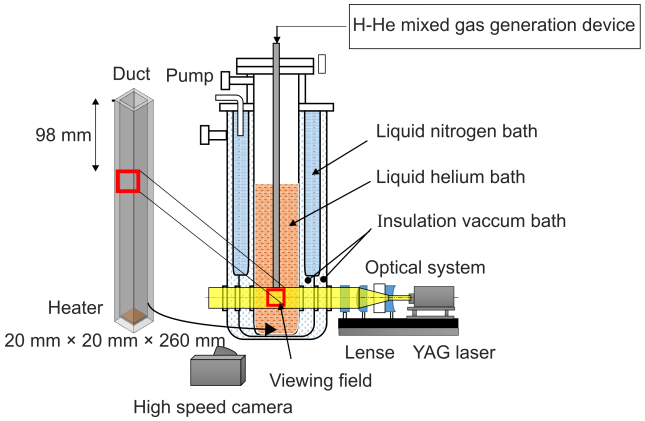

Fig. 1: Schematic view of experimental settings [11].

spouting pressure. The hydrogen particles are generated in the liquid helium. We adopted a mixing ratio of He:H_2 = 40:1 and a spouting pressure 20 kPa. Additionally, the injection is carried out just above the λ point, and then the bath temperature is decreased. In this study, we adopted the particle tracking algorithm developed by Crocker *et al.* [13]. The particle size, d, ranges from 5 to 40 μm [11]. We do not classify the size of the particles but analyze the motion of all particles.

3 Analysis Method

In principle, the curvature κ is a purely geometrical quantity and contains no dynamical information about the trajectory. However, the curvature can be written in terms of the temporal derivatives of the positions along the trajectory. The instantaneous curvature can be expressed as $\kappa = a_n/u^2$ [14] utilizing the Frenet formulas, where a_n is the magnitude of the normal acceleration, and u is the velocity, as shown in Fig. 2.

Also, the curvature is represented by $\kappa = |\mathbf{u} \times \dot{\mathbf{u}}|/|\mathbf{u}|^3$, where $\mathbf{u}$ is the vector of the velocity u. We use the PTV algorithm [13] to calculate the velocity and acceleration of the particles. The velocity and acceleration are calculated by

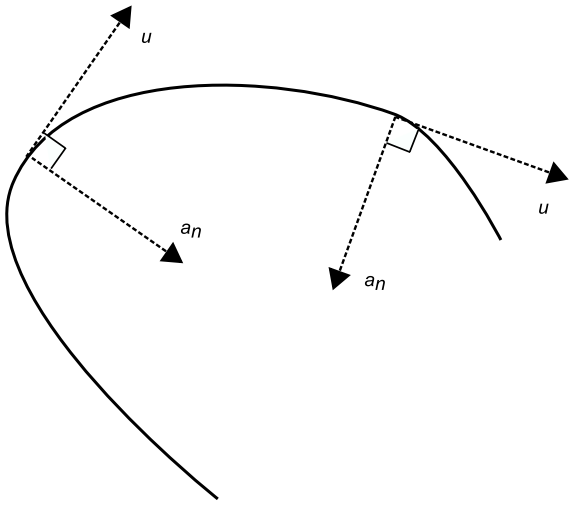

Fig. 2: Example of particle trajectory (solid line), Lagrangian velocity, and normal acceleration.

the numerical derivative with the central difference method. The uncertainly is $O(\Delta t)$ for velocity and $O(\Delta t^2)$ for acceleration.

The distribution of κ has been studied in classical turbulence [9][14]. The PDF of κ ($P(\kappa)$) demonstrates the two power-law regions where the high and low curvature regions have corresponding PDFs of $P(\kappa) \propto \kappa^{-5/2}$ and $P(\kappa) \propto \kappa$, respectively. Xu et al. [9] reported that this feature could be understood by the Gaussian property of random variables but not turbulent small-scale statistics. As is well known, the velocity fluctuation in classical turbulence closely mimics the Gaussian property. In addition, the velocity fluctuations (u_x, u_y, u_z) in HIT are independent of one another, then the magnitude $u^2 = u_x^2 + u_y^2 + u_z^2$ should follow a chi-squared distribution with degree of freedom three. When $\kappa \to \infty$, or $u \to 0$, the PDF of κ follows the distribution of u^{-2} with the assumption of finite a_n in this limit, suggesting a power-law with an exponent of $-5/2$. Similarly, the power-law scaling of $\kappa \to 0$ is derived. The PDF of curvature scales like the PDF of a_n as $a_n \to 0$ with the assumption that the components of a_n are independent Gaussian random variables. It is a reasonable approximation for small values of a_n, and the PDF of a_n^2 then follows a chi-squared distribution with a degree of freedom of two because the normal acceleration is confined to the plane orthogonal to the velocity vector. In the case of $\kappa \to 0$, the PDF of κ follows the distribution of a_n as $a_n \to 0$, then the power-law with an exponent of one is derived [9].

Moreover, the PDF of curvature in 2D case is also discussed. Since the PDF of velocity fluctuations and a_n near zero can be approximated as a quasi-Gaussian distribution, then the power-law of PDFs are derived as $P(\kappa) \approx \kappa^{-2}$ and $P(\kappa) \approx \kappa^0$ in $\kappa \to \infty$ and $\kappa \to 0$, respectively, using Taylor's expansion. The following equation approximates the PDF of curvature with the

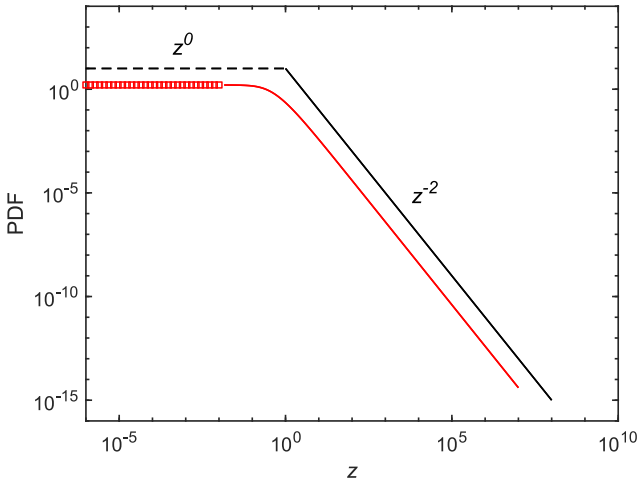

Fig. 3: PDF of curvature. The solid red line is Eq. (2), and the red squares are the asymptotic value of $z \to 0$. Solid and dotted black lines are z^{-2} and z^0, respectively.

dimensionless parameter $z = \kappa\sigma_u^2/\sigma_a$.

$$\begin{aligned} P(z) &= \int_0^\infty u^2 \exp\left(-\frac{a_n^2}{2}\right) \exp\left(-\frac{u^2}{2}\right) du^2 \\ &= \frac{1}{\sqrt{2\pi}z^2}\left(1 - \sqrt{\frac{\pi}{2}}\frac{1}{2z}\exp\left(\frac{1}{8z^2}\right)\mathrm{erfc}\left(\frac{1}{2\sqrt{2}z}\right)\right) \end{aligned} \tag{2}$$

where σ_u and σ_a are the standard deviations of velocity and the acceleration, respectively: erfc is the complementary error function.

$$\mathrm{erfc}\left(\frac{1}{2\sqrt{2}z}\right) = \frac{2}{\sqrt{\pi}}\int_{1/2\sqrt{2}z}^\infty \exp\left(-t^2\right) dt \tag{3}$$

The PDF of curvature in two dimensions has been reported by Yang et al. [10]. They evaluated the distribution of magnetic field line curvature by numerical simulation. The analytical solution of the PDF is derived for the first time in this paper.

Equation (2) is plotted as a red line in Fig. 3. The solid and dotted black lines represent the power-law relation of z^{-2} and z^0, respectively. Due to the numerical convergence, the PDF can be calculated by Eq. (2) in the range of $10^{-2} < z$. The red square dots denote the value of 1.6, which is the asymptotic value of Eq. (2) as $z \to 0$.

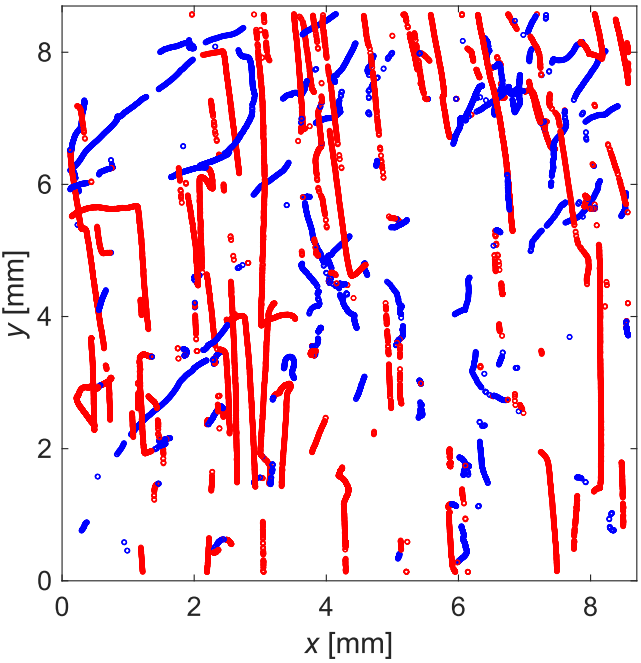

Fig. 4: Example of the trajectories in the case of $T = 2$ K with $q = 310$ W/m^2. Red circles represent the trajectories having positive averaged velocity. Blue circles represent the trajectories having negative averaged velocity.

4 Resuls and Discussiton

A typical example of particle trajectories is plotted in Fig. 4. They are colored in blue and red according to the criteria mentioned below. A Lagrange trajectory has a finite length or steps n counted in the discrete time interval Δt. It is given by $3 \leq n \leq n_{\max}$. The maximum of $n_{\max}$ is $O(10^3)$ in the present experiment. Along each Lagrange trajectory, the mean vertical velocity $\langle v_y \rangle_L$ is calculated by

$$\langle v_y \rangle_L = \frac{1}{n_{\max}} \sum_{i=1}^{n_{\max}} v_y(i\Delta t) \tag{4}$$

where $v_y(t)$ is the instantaneous velocity at time t. When $\langle v_y \rangle_L$ is positive, the trajectory is colored in red, and it is colored blue for negative $\langle v_y \rangle_L$. It is noted that the particle velocity is not always positive inside the red trajectory nor negative in the blue trajectory. In Fig. 4, where the temperature is 2K, the red trajectories tend to be long, but the blue trajectories are short. Furthermore, the red trajectories correspond to straight lines but blue trajectories are complicated. These features are consistent with the observation in previous research [5][15]. It should be emphasized that our defined red and blue trajectories do not always represent the particles carried by the normal and superfluid (or quantum vortex). Along one red trajectory, some parts interact

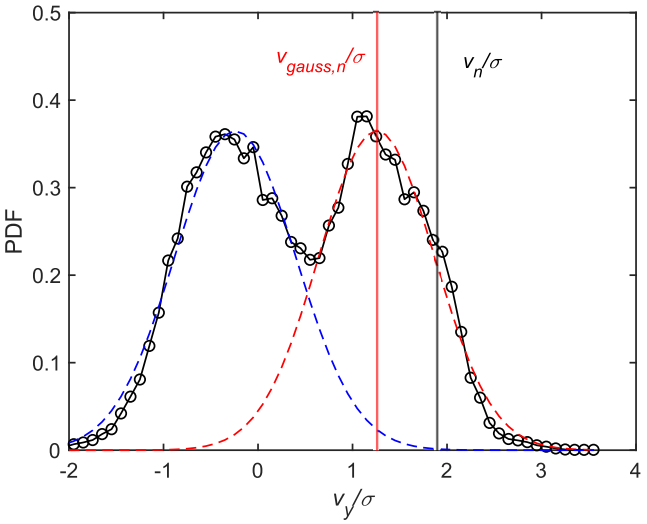

Fig. 5: PDF of vertical velocity component for the case of $T = 2$ K with $q = 470$ W/m^2. The bimodal PDF is approximated by two Gaussian profiles denoted by two dashed lines. The solid red line is the mean value v_y, the mean of the positive Gaussian fitting. The solid black line is the normal fluid velocity calculated by the two-fluid model.

with the quantum vortex, and blue trajectory contains the interaction with normal fluid partially. In principle, it is impossible to separate the particle trajectory carried by normal fluid perfectly. In Fig. 5, the PDF of the vertical velocity v_y is calculated for the case of $T = 2$ K with $q = 470$ W/m^2, in which the vertical velocity is normalized by its standard deviation σ. The PDF has a bimodal distribution similar to previous studies [2][5]. This bimodal distribution is confirmed in almost all cases. The bimodal distribution is approximated by two Gaussian distributions denoted by the blue and red dashed lines in Fig. 5. Their mean values are expressed as $v_{gauss,s}$ and $v_{gauss,n}$, respectively. The red line is the positive mean value $v_{gauss,n}$, and the velocity v_n is calculated by the two-fluid model (Eq. (1)), which is indicated by the solid black line.

The bimodal distribution was not observed for $T = 2.1$ K; however, the positive peak always appears. This was also confirmed by previous study [16] for similar heat flux $q \approx 900$ W/m^2. The mean velocity $v_{gauss,n}$ was plotted against v_n as shown in Fig 6. Different colors represent various experimental conditions. Moreover, the solid line is given by $v_{gauss,n} = v_n$, and the dotted line is denoted by $v_{gauss,n} = v_n/2$. There have been discussions on the particle velocity in counterflow [2][12]: the previous studies are summarized in [5]. In the previous studies [2][5][8][12], the $v_{gauss,n}$ agrees with v_n. In this measurement, $v_{gauss,n}$ and v_n increase as the heat power becomes large, and $v_{gauss,n}$ locates between v_n and $v_n/2$.

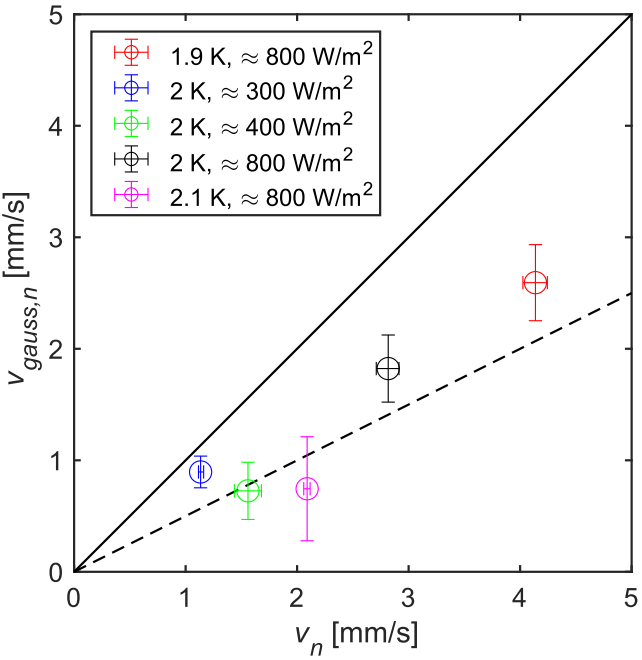

Fig. 6: Comparison of mean vertical velocity in experiments and the two-fluid model. The red color is $T = 1.9$ K with $q \approx 800$ W/m^2, blue is $T = 2.0$ K with $q \approx 300$ W/m^2, green is $T = 2.0$ K with $q \approx 400$ W/m^2, black is $T = 2.0$ K with $q \approx 800$ W/m^2, and magenta is $T = 2.1$ K with $q \approx 800$ W/m^2. The vertical error bar is the standard deviation in the each data sets. The horizontal error bar is the range of the theoretical normal fluid in the each data sets. The solid line represents $v_{gauss,n} = v_n$. The dotted line denotes $v_{gauss,n} = v_n/2$.

The PDFs of curvature normalized by the standard deviation σ_κ are plotted in Fig. 7. Different color symbols indicate the experimental conditions. They are $T = 1.9$ K with $q \approx 800$ W/m^2, $T = 2.0$ K with $q \approx 300$ W/m^2,$T = 2.0$ K with $q \approx 400$ W/m^2, $T = 2.0$ K with $q \approx 800$ W/m^2, and $T = 2.1$ K with $q \approx 800$ W/m^2 from the top, and each graph is shifted vertically not to avoid overlap. In the larger curvature region, the power-law is represented by the solid line with κ^{-2}. In the smaller curvature region, the power-law is given by the dashed line with κ^0. PDFs of curvature contain no signs of nonclassical behavior attributed to the quantum vortex in superfluid. When the curvature is normalized as $z = \kappa\sigma_u^2/\sigma_a$, the PDF is plotted in Fig. 8a. The gray squares are the asymptotic value of $z \to 0$, and the solid line is given by Eq. (2). The theoretical PDF of the curvature does not completely agree with the experimental results. They slightly deviate from Eq. (2) because it is derived under the assumption that the components of velocity and acceleration are independent Gaussian random variables and acceleration is noncorrelated with velocity. However, the acceleration usually has a large intermittent value, and

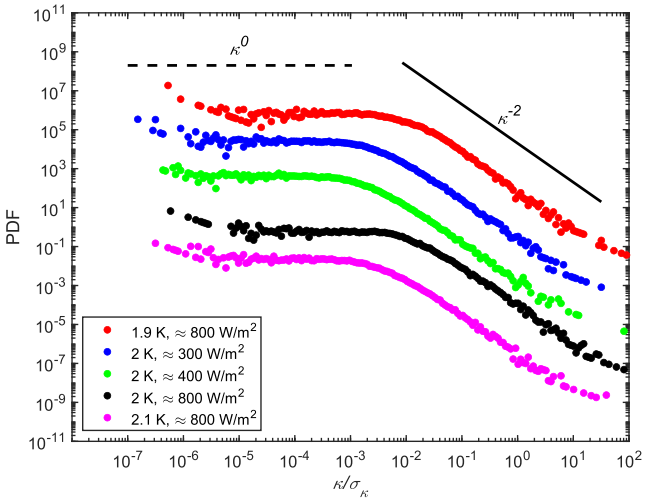

Fig. 7: PDF of curvature normalized by the standard deviation. The graphs of $T = 1.9$ K with $q \approx 800$ W/m^2, $T = 2.0$ K with $q \approx 300$ W/m^2, $T = 2.0$ K with $q \approx 400$ W/m^2, $T = 2.0$ K with $q \approx 800$ W/m^2, and $T = 2.1$ K with $q \approx 800$ W/m^2 (from the top) are shifted vertically to avoid overlap. The dotted black line represents the κ^0. The solid black line is given by the κ^{-2}.

its PDF indicates a long tail. In addition, the acceleration, and velocity can be correlated. Therefore, this assumption is not completely satisfied for the motion of particles in thermal counterflow.

For further analysis, the curvature PDF is divided into three regions: low, medium, and high curvature regions as described in Fig. 8b. This classification does not contain any physical meaning but is defined as the probability that each region is equal for convenience. In the low curvature region, the PDF is almost constant, or the power law is κ^0, and in the high curvature region, the PDF corresponds to the relation κ^{-2}. The medium region is located between these two power-law regions. A typical example of the PDF is plotted in Fig. 8b, where the low and the high curvature PDFs are given by $\kappa/\sigma_\kappa < 1.5 \times 10^{-3}$ and $6.0 \times 10^{-3} < \kappa/\sigma_\kappa$, respectively.

The histogram of particles is plotted in Fig. 9 as a function of curvature and vertical velocity. Following the definition, as described in Fig. 8b, the curvature is divided into three regions. The histogram indicates the high probability in the medium curvature region where the positive vertical velocity is dominant. Around a small vertical velocity of $v_y \simeq 0$, the particle motion indicates the high curvature. From these observations, we understand that the vertical velocity has different characteristics depending on the curvature. Then the vertical velocity is averaged in each region. In other words, the vertical velocity is

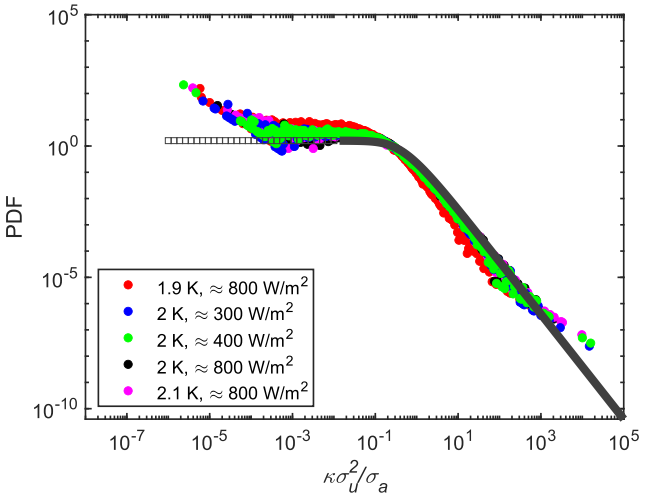

(a)

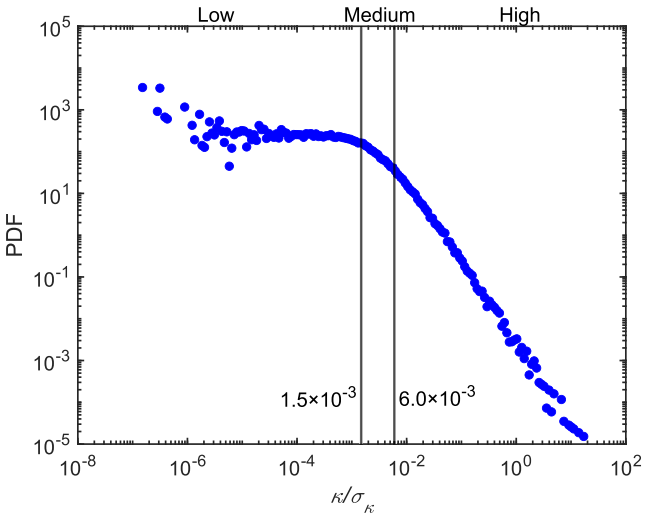

(b)

Fig. 8: (a)PDF of normalized curvature $z = \kappa\sigma_u^2/\sigma_a$. Gray solid line represents Eq. (2), and the gray square line signifies the value when the $z \to 0$. The color symbols are the same as in Fig. 7. (b) PDF of curvature is divided into the high, medium, and low regions for the $T = 2.0$ K with $q = 310$ W/m^2. Blue circles denote the PDF of curvature, the left solid line is the threshold between the low and medium region, and the right solid line is the threshold between the high and medium region.

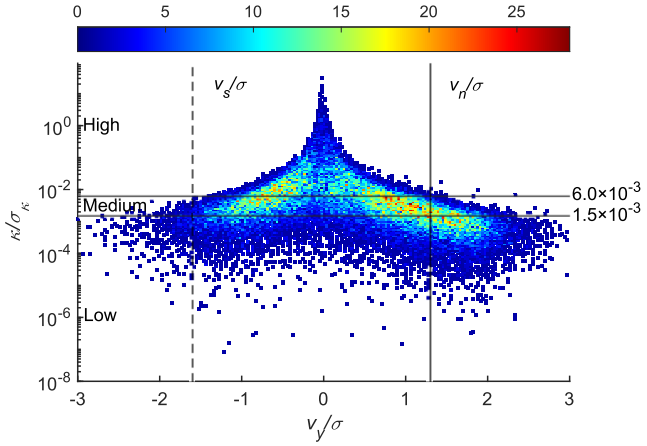

Fig. 9: Histogram of particles as a function of y direction velocity and curvature in the case of $T = 2.0$ K with $q = 310$ W/m^2. The lower solid line represents the threshold between the low and medium regions, and the solid upper line signifies the threshold between the high and medium regions. The left dotted line denotes the theoretical superfluid velocity divided by the standard deviation of the vertical velocity and the right solid line is the theoretical normal fluid velocity divided by the standard deviation of the vertical velocity.

conditioned by the intensity of curvature, and it is usually called conditional sampling.

The vertical velocity is divided into high, medium, and low curvature regions, and their PDF is plotted in Fig. 10 for the case of $T = 2$ K with $q = 310$ W/m^2. The original PDF shows the bimodal distribution, but the positive and negative peaks are located close to each other. However, in the velocity conditioned by the low curvature region, there are two clearly separated peaks. The positive peak is given by $v_{gauss,n}/\sigma \simeq 1.5$, and the negative peak is denoted by $v_{gauss,s}/\sigma \simeq -1.0$. In the high curvature region, the profile is approximated by the Gaussian distribution. The PDFs of the horizontal velocity v_x normalized by the mean and standard deviation σ_x are plotted in Fig. 11. Moreover, the original velocity distribution near the core is fitted well using the Gaussian distribution. This feature has been observed in other research [3][17]. In addition, we found that the velocity in high curvature region is also approximated by the Gaussian distribution.

The particle velocities of v_x and v_y in the high curvature region are approximated by Gaussian distribution, and they are independent. Then the magnitude of the velocity $v_x^2 + v_y^2$ follows a chi-squared distribution with a degree of freedom two. When $\kappa \to \infty$ or $(v_x^2 + v_y^2) \to 0$, the PDF of κ follows the distribution of $(v_x^2 + v_y^2)^{-2}$ with the assumption of finite a_n in this limit. Therefore, the PDF of curvature has a power-law tail of -2 as expressed in

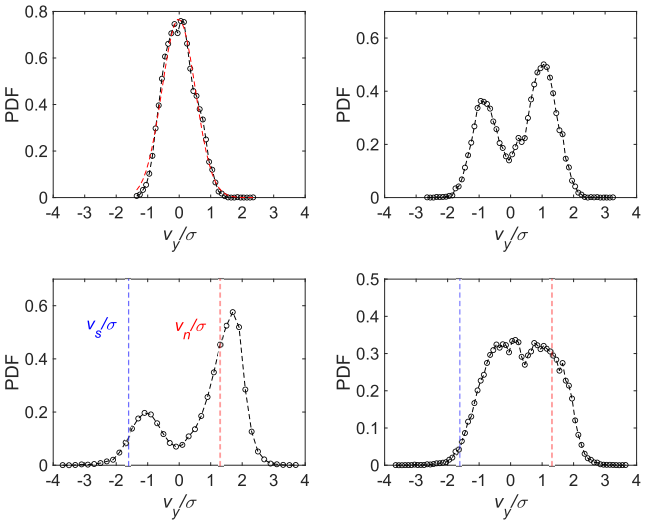

Fig. 10: PDF of vertical velocity divided by its standard deviation in high (top left), medium (top right), low (bottom left), and all (bottom right) curvature regions at $T = 2.0$ K with $q = 310$ W/m^2. In the high region, the dotted orange line represents the Gaussian fit.

Eq. (2). Similarly, the power-law of κ^0 is assumed because the normal acceleration could be thought of as Gaussian, and the velocity is finite in the limit of $\kappa \to 0$ or $a_n \to 0$, as expressed in Eq. (2).

The vertical velocity conditioned by the medium curvature region has a clear bimodal distribution even though the original PDF doesn't have a clear bimodal distribution in the case of $T = 2$ K with $q = 310$ W/m^2. The positive velocity peak is attributed to the conditional velocity in the medium curvature region but is only slightly affected by high curvature regions. The negative peak $v_{gaussu,s}$ also shows the different values depending on the curvature. In addition, negative and positive distributions are enhanced compared with the original PDF because, in the low heat flux, particles that feel stokes drag do not interact with vortices frequently and sometimes go down with quantum vortices. In the high heat flux, the vertical velocity PDF conditioned by the low curvature region does not have clear bimodal distribution, whereas the original PDF has a bimodal distribution. The tracer particles tend to move fast enough to detrap from the quantum vortices. Thus, the lower peak is located around the small positive value, and the vertical velocity PDF conditioned by the low curvature region does not have clear bimodal distribution for the high heat flux.

The vertical velocity calculated by the two-fluid model is plotted in Fig. 10. Additionally, the normal fluid velocity $v_{gaussu,n}$ agrees with v_n. Then the low curvature region along the Lagrange trajectory represents the laminar flow region where the particles are carried by Stokes drag. The negative particle

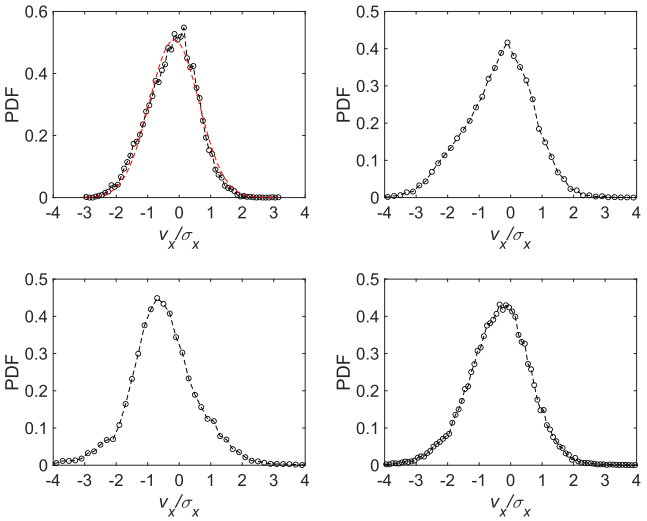

Fig. 11: PDF of horizontal velocity divided by the standard deviation in the high (top left), medium (top right), low (bottom left), and all (bottom right) curvature regions at $T = 2.0$ K with $q = 310$ W/m^2. In the high region, the dotted orange line represents the Gaussian fit.

velocity $v_{gaussu,s}$ does not agree with the two-fluid model but is close to v_s compared with original PDF.

The vertical velocity $(v_{gaussu,n})_{\text{Low}}$ conditioned by the low curvature region is plotted against the normal velocity v_n using the $*$ symbol, as shown in Fig. 12a. Furthermore, conditional normal fluid velocities are shown to be close to those of the two-fluid model, especially when the range v_n is below 2 mm/s. However, the conditional velocity still deviates from the original v_n in high-velocity regions. Next, we calculate the velocity difference $(v_{gaussu,n})_{\text{Low}} - v_{gauss,n}$ in Fig. 12b. Note that the data at $T = 2.1$ K with $q \approx 800$ W/m^2 is not included here because the vertical velocity shows no bimodal distribution. In addition, one of the samples in $q = 470$ W/m^2 is excluded since the original PDF does not have a clear bimodal distribution. It is found that the difference is large in $v_n < 2$ mm/s but small for $v_n > 2$ mm/s. Since the quantum vortex density L increases as the heat flux increases, the interaction between the tracer particles and quantum vortices frequently occurs. Thus, the particles move up in a zigzag pattern. Moreover, the vertical velocity PDF conditioned by the low curvature region tends to include these velocity components. Therefore, the difference between the original and conditional PDFs is small in the high heat flux.

We plot the examples of the high curvature points on the trajectories for $T = 2.0$ K with $q = 310$ W/m^2. The trajectories are extracted from Fig. 13, where the red points represent the upward motion. Along the trajectory, the

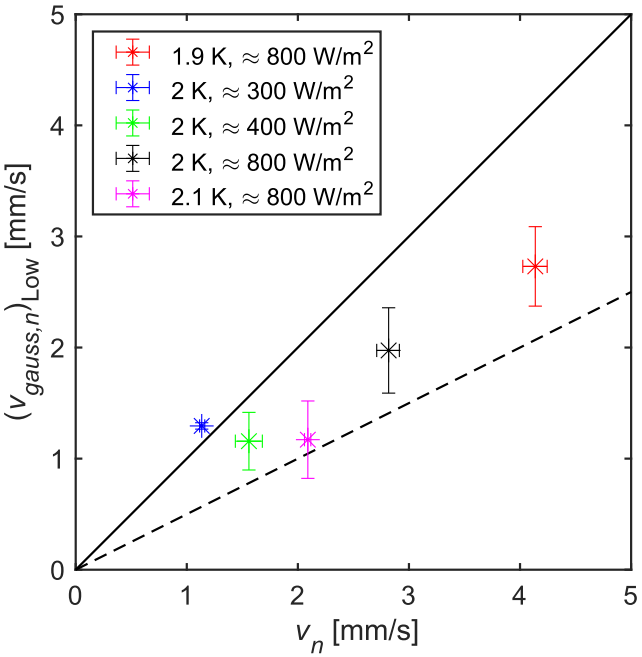

(a)

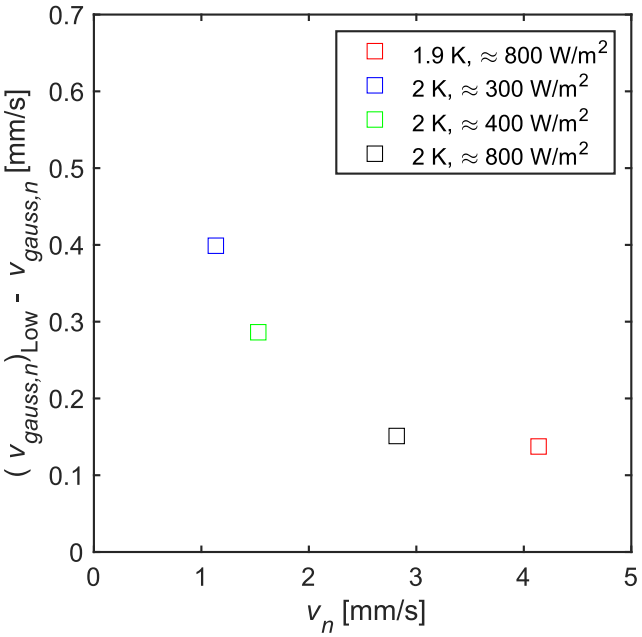

(b)

Fig. 12: (a) Gaussian fit value to the larger velocity peak in the low curvature region. The color and the error bar are the same with those of the Fig. 6. (b) Each squares represent difference between the mean value of Fig. 12a and Fig. 6. The color is the same with that of Fig. 6.

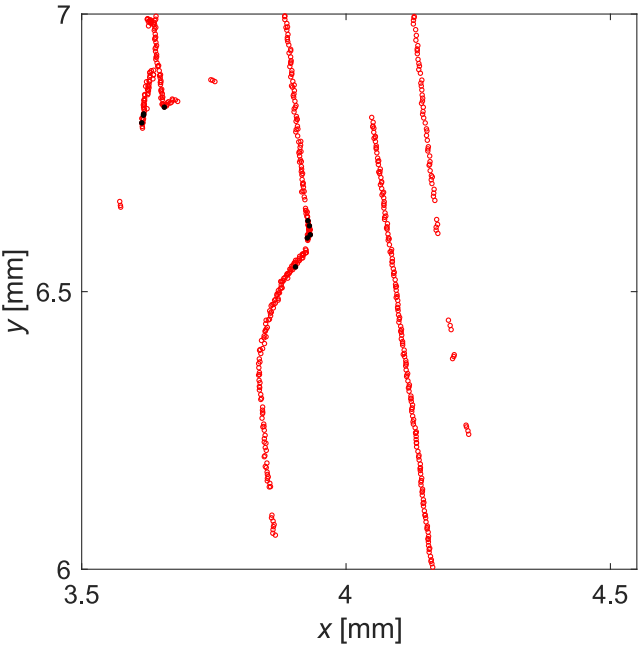

Fig. 13: An example of high curvature points on the trajectories for the case of $T = 2.0$ K with $q = 310$ W/m^2. Red trajectories are extracted from Fig. 4. Black points indicate the high curvature region, $7.0 \times 10^{-2} < \kappa/\sigma_\kappa$.

high curvature region ($7.0 \times 10^{-2} < \kappa/\sigma_\kappa$) is colored in black. As expected, the high curvature region indicates nonstraight motion or the point where the particle motion suddenly changes its direction, which could be due to the quantum vortex interaction.

5 Conclusion

In this study, we calculate the curvature of the 2D-Lagrangian trajectory in thermal counterflow using PTV. The Lagrange velocities (vertical component v_y and horizontal component v_x) are conditionally averaged by curvature values. Furthermore, results show that the trajectory exhibits a complex shape or a sudden change in the direction of the particle in the high curvature region. In addition, by removing the high curvature region from the trajectory and conditioning the vertical velocity in the low curvature region, we achieve a bimodal velocity distribution, thereby making the normal fluid velocity close to the value of the two-fluid model. Therefore, the quantum vortex tangled complex interactions are sufficiently separated based on the curvature in the low heat flux case. However, in the high heat flux condition, bimodal distribution does not tend to appear in the low curvature region although it is seen in the

original distribution. Both v_y and v_x have a Gaussian distribution with a zero-mean value in the high curvature region. Based on this experimental evidence, the PDF of curvature in the 2D case is analytically derived as a function of the dimensionless parameter $z = \kappa\sigma_u^2/\sigma_a$. It has the power-law scaling $\approx \kappa^{-2}$ in the high curvature region, and is confirmed in the present experiment.

Acknowledgments. This work was supported by JSPS KAKENHI Grant Numbers JP19H00747, JP19H00641. This work was also financially supported by JST SPRING, Grant Number JPMJSP2125. The author N. S. would like to take this opportunity to thank the "Interdisciplinary Frontier Next-Generation Researcher Program of the Tokai Higher Education and Research System." The experimental support by Mr. S.Waki was indispensable in our measurements.

Data Availability Statement. Data are available on reasonable request.

References

[1] G. P. Bewley, D. P. Lathrop, and K. R. Sreenivasan, Visualization of quantized vortices, Nature, **441**, 588 (2006)

[2] M. S. Paoletti, R. B. Fiorito, K. R. Sreenivasan, and D. P. Lathrop, Visualization of Superfluid Helium Flow, J. Phys. Soc. Jpn., **77**, 111007 (2008)

[3] M. La. Mantia and L. Skrbek, Quantum or classical turbulence?, Europhys. Lett., **105**, 46002 (2014)

[4] M. La. Mantia and L. Skrbek, Quantum turbulence visualized by particle dynamics, Phys. Rev. B, **90**, 014519 (2014)

[5] B. Mastracci and W. Guo, Exploration of thermal counterflow in He II using particle tracking velocimetry, Phys. Rev. Fluids, **3**, 063304 (2018)

[6] Y. Tang, S. Bao, and W. Guo, Superdiffusion of quantized vortices uncovering scaling laws in quantum turbulence, Proc. Natl. Acad. Sci. U.S.A., **118**, e2021957118 (2021)

[7] W. Kubo and Y. Tsuji, Statistical Properties of Small Particle Trajectories in a Fully Developed Turbulent State in He-II, J. Low Temp. Phys., **196**, 170 (2019)

[8] P. Švančara, D. Duda, P. Hrubcová, M. Rotter, L. Skrbek, M. La Mantia, E. Durozoy, P. Diribarne, B. Rousset, M. Bourgoin, and M. Gibert, Ubiquity of particle–vortex interactions in turbulent counterflow of superfluid helium. J. Fluid Mech., **911**, A8 (2021)

[9] H. Xu, N. T. Ouellette, and E. Bodenschatz, Curvature of Lagrangian Trajectories in Turbulence, Phys. Rev. Lett., **98**, 050201 (2007)

[10] Y. Yang, M. Wan, W. H. Matthaeus, Y. Shi, T. N. Parashar, Q. Lu, and S. Chen, Role of magnetic field curvature in magnetohydrodynamic turbulence, Phys. Plasmas, **26**, 072306 (2019)

[11] N. Sakaki, T. Maruyama, and Y. Tsuji, Statistics of the Lagrangian Trajectories' Curvature in Thermal Counterflow, J. Low Temp. Phys. (in press) (2022)

[12] T. V. Chagovets and S. W. Sciver, A study of thermal counterflow using particle tracking velocimetry, Phys. Fluids, **23**, 107102 (2011)

[13] We use particle tracking algorithm developed by John Crocker, Eric Weeks and David Grier.

[14] W. Braun, F. De Lillo, and B. Eckhardt, Geometry of particle paths in turbulent flows, J. Turbul., **7**, 1 (2006)

[15] M. La Mantia, Particle trajectories in thermal counterflow of superfluid helium in a wide channel of square cross section, Phys. Fluids, **28**, 024102 (2016)

[16] B. Mastracci, S. Takada, and W. Guo, Study of Particle Motion In He II Counterflow Across a Wide Heat Flux Range, J. Low Temp. Phys., **187**, 446 (2017)

[17] M. La Mantia, D. Duda, M. Rotter, and L. Skrbek, Lagrangian accelerations of particles in superfluid turbulence, J. Fluids. Mech., **717**, R9 (2013)